Magnetic Resonance Imaging Reveals Distinct Roles for Tissue Transglutaminase and Factor XIII in Maternal Angiogenesis during Early Mouse Pregnancy

Gadi Cohena, Ron Hadasa, Rachele Stefania, Amerigo Pagoto, Shifra Ben-Dor, Fortune Kohen, Dario Longo, Michal Elbaz, Nave Dekel, Eran Gershon, Silvio Aime, Michal Neeman

MRI reveals distinct roles for tissue transglutaminase and factor XIII in maternal angiogenesis during early mouse pregnancy

In Arterioscler Thromb Vasc Biol.

The definitive version is available at:
DOI: 10.1161/ATVBAHA.119.312832

MRI reveals distinct roles for tissue transglutaminase and factor XIII in maternal angiogenesis during early mouse pregnancy

Authors
Gadi Cohen[a,*], Ron Hadas[a,*], Rachele Stefania[b], Amerigo Pagoto[b], Shifra Ben-Dor[c], Fortune Kohen[a], Dario Longo[b], Michal Elbaz[d], Nave Dekel[a], Eran Gershon[d], Silvio Aime[b], Michal Neeman[a]

[a] Department of Biological Regulation, Weizmann Institute of Science, Rehovot, Israel 76100; [b] Department of Molecular Biotechnology and Health Sciences, University of Torino, Torino, Italy 10124; [c] Life Science Core Facilities, Weizmann Institute of Science, Rehovot, Israel 76100; [d] Department of Ruminant Science, Agricultural Research Organization, Bet Dagan, Israel 50250

Corresponding author
Michal Neeman;
Department of Biological Regulation
Weizmann Institute of Science
Rehovot, 76100 Israel
Email michal.neeman@weizmann.ac.il
Tel +972-8-9342487

Running title: MRI of transglutaminase during embryo implantation

*G.C. and R.H. contributed equally.

TOC category: Basic, Translational, and Clinical Research

TOC subcategory: Developmental Biology, Angiogenesis and Vascular Biology

Word count: 7264

Total number of figures and tables: 6 figures; 5 supplementary figures and 2 supplementary tables.

Abstract

Objective: The early embryo implantation is characterized by enhanced uterine vascular permeability at the site of blastocyst attachment, followed by extracellular-matrix (ECM) remodeling and angiogenesis. Two transglutaminase (TG) isoenzymes, tissue TG (TG2) and factor XIII (FXIII), catalyze covalent cross-linking of the ECM. However, their specific role during embryo implantation is not fully understood.

Approach and Results: For mapping the distribution as well as the enzymatic activities of TG2 and FXIII towards blood-borne and resident ECM substrates, we synthetized selective and specific low molecular weight substrate analogs for each of the isoenzymes. The implantation sites were challenged by genetically modifying the trophoblast cells (TC) in the outer layer of blastocysts, to either overexpress or deplete TG2 or FXIII, and the angiogenic response was studied by dynamic contrast-enhanced-(DCE) MRI. DCE-MRI revealed a decrease in the permeability of decidual vasculature surrounding embryos in which FXIII were overexpressed in TC. Reduction in decidual blood volume fraction was demonstrated when either FXIII or TG2 were overexpressed in embryonic TC and was elevated when TC were depleted of FXIII. These results were corroborated by histological analysis.

Conclusions: In this study we report on the isoenzyme-specific roles of TG2 and FXIII during the early days of mouse pregnancy and further reveal their involvement in decidual angiogenesis. Our results reveal an important MRI-detectable function of embryo derived TG2 and FXIII on regulating maternal angiogenesis during embryo implantation in mice.

Abbreviations:

Bovine serum albumin (BSA); Collagen IV (CIV); Dynamic contrast-enhanced- MRI (DCE-MRI); Extracellular-matrix (ECM); Factor XIII (FXIII); Fractional blood volume (fBV); Green fluorescent protein (GFP); Implantation sites (IS); Intravenously (IV); Single guide RNA (sgRNA); Substrate analog (SA); Permeability surface area product (PS); Transglutaminase (TG); Tissue TG (TG2); Trophoblast cells (TC).

Introduction

Implantation of mammalian blastocysts into the uterine endometrium involves a series of precisely synchronized events that are influenced by interactions between the embryo and its maternal environment [1]. Upon attachment, during the fifth day of mouse pregnancy [2], the embryo invades the maternal uterine epithelium at the anti-mesometrial pole of the implantation site (IS) [3,4]. Consequently, uterine stromal cells rapidly proliferate and differentiate to form the decidua [5], providing a permissive and controlled environment for the invasion of embryonic trophoblast cells (TC) [6,7]. Concurrently, maternal blood vessels expand in number and diameter, and uterine vascular permeability increases locally around the IS [8,9]. These changes enabled invasive detection of embryo IS at an early stage by leakage of intravenously (IV) administered vital dyes, and non-invasive detection of embryo implantation by Dynamic contrast-enhanced (DCE)-MRI [10,11].

Embryo implantation failure is the primary cause for the low rate of success of *in vitro* fertilization programs [5]. Impaired uterine hyper-permeability has been proposed as a cause for implantation failure in humans [12]. Several complications of pregnancy, such as preeclampsia and intrauterine growth restriction, have been attributed to disturbances in early uterine blood supply [13] or impaired TC invasion of the placental bed spiral arterioles later in pregnancy [14].

Transglutaminases (TG) catalyze covalent cross-links between proteins in various processes associated with angiogenesis and ECM remodeling, such as wound healing, cancer invasion and embryo implantation [15]. The most prominent TG isoenzymes, are tissue TG (TG2), that serves as a signaling molecule aside from its cross-linking activity [16,17] and factor XIII (FXIII), which participates in the final stage of the coagulation cascade, by catalyzing cross-links between fibrinogen or fibrin molecules [18,19]. In addition to fibrinogen, several ECM glycoproteins, such as collagen, were found to be cross-linked by FXIII [20–22].

We previously reported substrate analogs (SAs) for both TG2 and FXIII, labeled with either Gd(III)-DOTA or a fluorescent dye were designed to investigate their role in mouse models of tumor xenografts and blood clotting [23,24]. Selective peptide substrates specific for either TG2 or FXIII were identified by a Phage display screen [25]. Given that both TG2 and FXIII are expressed at the embryo-maternal surface during early development [17,26], the aim of this study was to determine the distinct roles of TG2 and FXIII in maternal vascular development during embryo implantation in mice. To do so, we successfully synthesized SAs for the two enzymes [27,28] demonstrating a highly selective and specific reactivity to their respective TG isoenzymes. TG2 and FXIII activities were further confirmed by determining the synthetized SAs distributions on IS sections. The contribution of embryo derived TG activity was assessed by genetically modifying the blastocyst trophectoderm, in which the outer TC underwent lentiviral infection to overexpress TG2 or FXIII or using CAS-9 endonuclease to deplete their expression.

Briefly, DCE-MRI of surrogate pregnant mice carrying embryos with FXIII overexpressed TC, revealed a significant decrease in blood volume at the IS regions, while reduction in vessel permeability was demonstrated in embryonic TC overexpressing either FXIII or TG2. Furthermore, IS with FXIII-depleted TC displayed a significant increase vascular permeability, while vasculature changes were not detected in IS of TG2 depleted embryos . These MRI results demonstrate the distinct roles of embryo derived TG2 and FXIII in maternal vascular remodeling during embryo implantation.

Materials and Methods

The data that support the findings of this study are available from the corresponding author upon reasonable request.

Synthesis and characterization of the SAs F11-B and T29-B.

All materials were purchased from Sigma-Aldrich Israel Ltd, Rehovot, Israel unless indicated otherwise. T29: REQLYLYNVFS and F11: DQMMLPWPAVKL sequences were based on a phage-displayed random peptide library screen [25,27,29]. Peptides were synthetized by a Liberty CEM microwave peptide synthesizer (CEM SRL, Bergamo, Italy) by standard Fluorenylmethyloxycarbonyl (Fmoc) strategy using H-Rink amide ChemMatrix® resin (35-100 mesh particle size) as solid support on a 0.1 mmol scale. Peptide coupling was performed in dimethylformamide (DMF) using the amino acid (4 equivalent), PyBOP (Benzotriazol-1-yloxy)tripyrrolidinophosphoniumhexafluorophosphate, 4 equivalent) and N,N-Diisopropylethylamine (DIPEA), 8 equivalents. The synthesis of T29-B also included additional conjugation with 8-amino 3,6-dioxaoctanoic acid linker at the terminal amino group in order to introduce a spacer between the targeting peptide and biotin. After the automatic synthesis, the resin-peptide (~0.1 mmol of NH2 –terminated peptide) was mixed with a DMF solution of biotin-N-hydroxysuccinimide (0.3 mmol, 0.102 gr) and DIPEA (0.8 mmol, 0.143 ml). The mixture was stirred at room temperature for 12 h and the resin was thoroughly washed with DMF, dichloromethane, and diethylether. After cleavage and deprotection with trifluoroacetic acid (TFA) /Phenol/water/triisopropylsilane/ethanedithiol (82.5:5:5:5:2.5, v/v), the peptide was precipitated and the solid was washed with diethyl ether. The solid was lyophilized to give the final product (68 mg, yield 36%, and purity 80% for T29-B and 60 mg, yield 33%, purity 85% for F11-B). Analytical HPLC-MS (Fig I.A, upper part for T29-B; and Fig I.B, upper part for F11-B) was carried out on a Waters Fraction Lynx auto-purification system equipped with micromass ZQ ESI(+) ionization mode and dual-λ detectors, using Waters Atlantis RP-C18 column, 5 µm, 4.6 mm x 150 mm and H_2O/0.1% TFA and CH_3CN/0.1% TFA as eluents. Method: initial condition 15% CH_3CN/0.1% TFA, linear gradient 15-30% CH_3CN/0.1% TFA over 12.5 min, 30-100% CH_3CN/0.1% TFA over 17.5 min, flow rate 1 ml/min, detection UV at 220nm. T29-B: t_R= 18.4 min ESI-MS (m/z): observed: 959.6 $[M+2H]^{2+}$, 1918.6 $[M+H]^+$ (Fig I.A, insert); calculated for $C_{82}H_{131}N_{19}O_{20}S$: 960.0, 1918.1. F11-B: t_R= 22.0 min, ESI-MS (m/z): observed: 600.3 $[M+3H]^{3+}$, 827.5 $[M+2H]^{2+}$, 1655 $[M+H]^+$ (Fig I.A, insert); calculated for $C_{76}H_{119}N_{17}O_{18}S_3$: 600.7, 900.6, 1655. Absorbance at 280 nm of T29-B (Fig I.A, lower part) and F11-B (Fig I.B, lower part) was used to calculate their concentration, whereas their purification was carried out by preparative HPLC using a buffered solution of ammonium acetate as eluent.

TG activity assay

TG activity was determined as previously reported [23,24] using solid-phase microtiter plates coated with N,N'-dimethylcasein (20 mg/mL; overnight at 4^0C). The unbound N,N'-dimethylcasein was discarded and the wells were blocked with Tris [tris(hydroxymethyl)aminomethane)] 0.1 mM, pH=8.5 supplemented with 3% bovine serum albumin. Before being added to the reaction, 10 µg FXIII (Enzyme Research Laboratories, South Bend, IN) was activated by incubation with 40 U/ml NIH human Thrombin for 45 min at room temperature. The cross-linking reactions of SAs were performed in a total volume of 200 µL containing 1 mM of SAs, 0.1M $CaCl_2$, 0.1 M Tris, 0.05 M Dithiothreitol and gpTG2 13 µg (≥1.5 U/mg) (Fig I.C) or FXIII (Fig I.D). Reactions were carried out while incubated at 37^0C for 1 h and were stopped by washing with 50mM Ethylenediaminetetraacetic acid (EDTA). The incorporated SAs were detected using 1:150 streptavidin-alkaline phosphatase with phosphatase substrate. Kinetic measurements of absorbance at 405 nm were determined at 15-sec intervals for a period of 5 min (VICTOR2; Wallac, 1420 Multilabel counter; Winpact Scientific Inc, Irvine, CA). Relative activity of TG2 is expressed as units of absorbance. (*N*-(5-Aminopentyl)biotinamide (Cadaverine-B; BP; Pierce, Rockford, IL), nonspecific TG substrate, was used as a positive control. As negative control, the reaction mixture contained EDTA (50 mM) instead of $CaCl_2$. Measurements were analyzed as the ratio between the

absorbance intensity of the reacted peptide to the absorbance intensity of the negative control. The values are mean ± SD (n=3). * $p<0.05$ vs F11-B; ** $p<0.05$ vs T29-B.

Immunohistochemistry

Uterus sections containing hemizygote embryos of Myr-Venus on E5.5 (Figs 1A,E) or E6.5 (Figs 2A,E) or surrogate ICR mice carrying embryos with transgenic TC on E6.5 (Figs II and V) were fixed in 4% paraformaldehyde and later embedded in paraffin blocks and sectioned serially at a 4 µm thickness. The paraffin sections were deparaffinized with xylene for 15 min, followed by sequential ethanol hydration and double-distilled water. Sections were then washed with PBS followed by antigen retrieval in Citrate (pH 6.0) or EDTA (pH 8.5) buffer using a pressure cooker at 125ºC for 3 min. Thereafter, samples were blocked and permeabilized by 20% horse serum and 0.2% Triton X-100 in PBS. The following primary antibodies were added to the samples and incubated overnight at 4^0C: mouse anti TG2, mouse anti FXIII (Abcam, Cambridge, UK) and goat anti GFP, rat anti CD34 (CEDARLANE, Burlington, NC), anti CIV antibody biotin conjugate (600-406-106, Rockland Immunochemicals Inc., Limerick, PA) and rabbit anti fibrinogen (ab34269; Abcam, Cambridge, UK). Next, slides were washed with PBS and incubated with the appropriate secondary antibodies diluted 1:150 in PBS for 45 min at room temperature: CY5, Cy3 or Cy2-conjugated streptavidin, Cy3 anti mouse (Jackson Immunoresearch Laboratories, West Grove, PA) or Alexa488 anti goat. Please see the Major Resources Table in the Supplemental Material for additional information. Cell nuclei were fluorescently stained with DAPI. The fluorescent signal was detected in X5, X10 or X20 magnifications using a fluorescent microscope (Zeiss Axioscope II, Yena, Germany, Simple PCI software). Images were processed as described earlier using ImageJ software.

Histological analysis of TG2 and FXIII activities

Substrate analogs T29 for TG2 and F11 for FXIII were synthetized based on a phage-displayed random peptide library screen [25,27,29]. Sections of mice uteri were used for histological mapping of TG2 and FXIII activities, according to the method described by Kawamoto with slight modifications [30,31]. Briefly, 8-12 weeks old C57bl/6J female mice (Envigo, Jerusalem, Israel) were mated with Myr-Venus [32] homozygote males in order to produce hemizygote embryos for Myr-Venus. On E5.5 or E6.5 the dams were injected IV with 0.1 mM of T29-B or F11-B dissolved in PBS with 3% DMSO. 45 min after injection mice were sacrificed and their uteri were freeze-embedded with optimum cutting temperature compound (Tissue-Tek, Sakura Finetek, CA). Fifteen-µm-thick sections were prepared from the frozen specimen block using a cryomicrotome (Leica Co. Ltd., Wetzlar, Germany).

Uteri sections of untreated C57bl/6J pregnant mice were used for detecting TG2 and FXIII activities by *in situ* administration of the SAs. Specificity of the SAs was also observed *in situ* by inhibiting TG activity with iodoacetamide. Sections were air dried and then blocked with 1% BSA at room temperature for 30 min. Sections were then incubated for 60 min at 37^0C in the substrate reaction solution, consist of 100 mM tris(hydroxymethyl)aminomethane (Tris; pH 8.0), 1 mM dithiothreitol 5 mM $CaCl_2$ and T29-B or F11-B at the final concentration of 10 µM. Non-specific activity of the SAs was detected by adding 1 mg/ml of iodoacetamide to the reaction solution. Enzymatic reaction was stopped using 50 mM ethylenediaminetetraacetic acid (EDTA). Following fixation, all sections were blocked and incubated with Cy3-streptavidin (Jackson Immunoresearch Laboratories, West Grove, PA). IS with Myr-Venus hemizygote embryos were further treated with 1:500 goat anti-green fluorescent protein (GFP; Abcam, Cambridge, UK) diluted in 20% horse serum and 0.2% Triton X-100 overnight at 4^0C. Sections were treated with Alexa488 anti-goat (Abcam, Cambridge, UK) and cell nuclei and later stained by DAPI. Samples were observed under a fluorescence microscope using X10 or

X20 magnifications (Zeiss Axioscope II, Yena, Germany, Simple PCI software). Vessel density was determined with Fluorescence images of anti-CD34 staining[11] using ImageJ software (Wayne Rasband, NIH, MD). In brief, under identical conditions the fluorescence intensity of the stained area from the total IS area was measured in absolute counts after applying an automatic threshold. Fluorescent intensity outside the vessel area were masked and excluded from calculation. The average fluorescence intensity inside the IS region was calculated by measuring the ratio of fluorescence signal intensity to the area of region of interest.

Lentiviral vectors design and production

Lentiviral vectors were constructed to induce expression of mouse TG2 or mouse FXIII (see supplementary Table I for gene identifiers of TG2 and FXIII). Mouse TG2 and mouse FXIII were isolated from uterine cDNA restriction-free cloning using primers containing complementary overhangs to the designated target vector LV-GFP (supplemental Table II). The purified PCR products were cloned into the lentiviral expression vector, LV-GFP (provided by Dr. Oded Singer, Weizmann Institute of Science, Israel). To efficiently knock-out of TG2 or FXIII, two single guide RNA (sgRNA) targeting TG2 or FXIII were used (supplemental Table II). The guides were chosen to maximize on target scores and minimize off-target scores using several CRISPR designing tools, including: the MIT CRISPR design tool [33] and sgRNA Designer, Rule Sets 1 and 2 [34,35], in both the original sites and in the Benchling implementations websites (www.benchling.com), SSC[36], and sgRNA scorer[37], The sgRNA guide sequences were cloned into lentiCRISPR v2 lentiviral vector (Dr. Igor Ulitsky and Dr. Yoav Lubelsky, Weizmann Institute, Israel) according to Sanjana et al [38] with slight modifications. Briefly, oligonucleotides for the TG2 or FXIII sgRNA guide sequences were phosphorylated using T4 PNK (NEB, Ipswich, MA) for 30 min at 37°C, then annealed by heating to 95°C for 5 min and cooled down to 25^0C at 5^0C/min. The lentiCRISPR v2 vector and the annealed oligos were then supplemented with FastDigest BsmBI (Thermo Fisher Fermentas, Waltham, MA) and T7 ligase (NEB, Ipswich, MA) by six cycles of 5 min at 37°C followed by 5 min at 23^0C. The ligation reaction was next treated with PlasmidSafe exonuclease (NEB, Ipswich, MA) for 30 min at 37^0C. Recombinant lentiviruses were produced by transient transfection [39] in HEK293FT cells (Invitrogen, Carlsbad, California, U.S.A) using 3 envelope and packaging plasmids and one of the following viral construct: TG2-LV-GFP (TG2 overexpression), TG2-CRISPR-v2 (TG2 depletion), FXIII-LV-GFP (FXIII overexpression), FXIII-CRISPR-v2 (FXIII depletion), Control-LV-GFP (LV-GFP vector without insert) or Control-CRISPR-v2 (lentiCRISPR v2 vector without insert). Viral supernatants were harvested 48 h post-transfection and filtered through a 0.45 µm pore cellulose acetate filters and concentrated by ultracentrifugation. Lentiviral supernatant titers were determined by Lenti-X p24 Rapid Titer Kit (supplemental Table II) according to manufacturer's protocol (Takara Bio USA, Inc. California, U.S.A).

TG2 and FXIII overexpression validation

Validation was conducted using Western Blot analysis (Fig II.D). HEK293FT cells at 90% confluence were seeded in a 6 well plate. The next day cells were infected by the constructed lentivirus: TG2-LV-GFP, FXIII-LV-GFP or Control-LV-GFP. The following day cells were harvested and 50 µg of cell lysates were separated by 12% polyacrylamide SDS-PAGE. Protein fractions were transferred on ice to nitrocellulose membranes (100 V for 1 h; Whatman, Dassel, Germany). Membranes were blocked by incubation with 20 % BSA and 0.1% Tween-20 in Tris buffered for 2 h at room temperature. Western blot analysis was performed was performed by incubating first with primary mouse monoclonal anti-TG2 or anti-FXIII antibodies (1:500; Abcam, Cambridge, UK), followed by secondary anti-mouse horseradish peroxidase conjugate

(Jackson ImmunoResearch, West Grove, PA) and visualized with ECL (Pierce, Rockford, IL). In addition, blastocysts from all three groups were stained by whole-mount incubation with antibodies against TG2 (Fig II.C) and FXIII (Fig II.D), stained with specie specific secondary antibodies, Cy3 anti mouse (1:1000; Jackson Immunoresearch Laboratories, West Grove, PA), counterstained with 4′,6-diamidino-2-phenylindole (DAPI; 1:1000; Vector Laboratories, Burlingame, CA), subsequently mounted in mineral oil. Images were taken using spinning disk 386 confocal microscope using X40 magnification (Zeiss, Cell observer SD, Yena, Germany).

Generation of surrogate mice carrying embryos with genetically modified TC

All animal experiments were approved by the Animal Care and Use Committee of the Weizmann Institute (Approval numbers: 20510915-2 and 26130416-1). Follicle development was induced by pregnant mare's serum gonadotropin (5 IU sc; PMSG; Sigma-Aldrich, Rehovot, Israel) in 21 days old wild type ICR female mice (Harlan, Jerusalem, Israel). After 48h ovulation was induced by human chorionic gonadotropin (5 IU sc; hCG; Sigma-Aldrich, Rehovot, Israel). PMSG/hCG-treated female mice were housed overnight with wild-type ICR males and the next morning the presence of a vaginal plug was examined (defined as embryonic day 0.5; E0.5). The female mice were sacrificed three days later, and embryos at the morula or blastocyst stage were flushed out of the uteri. The embryos were incubated in potassium-supplemented simplex optimized medium (KSOM) to expand the blastocysts and their Zona pellucida was removed in acidic Tyrode's solution [40]. Next, 20-40 embryos were incubated with lentiviruses in KSOM for 6 h at 37^0C and subsequently were washed four times[7]. Prior to embryo transfer blastocysts (Fig II.A) expressing control vector or overexpressing TG2 or FXIII, were visualized for GFP expression. Using Non-surgical embryo transfer kit (NSET, ParaTechs, Lexington, KY), 10 blastocysts were transplanted into E2.5 pseudopregnant ICR female mouse. Pseudopregnancy was achieved by mating the wild-type ICR females with vasectomized males of proven sterility.

DCE MRI studies

DCE-MRI experiments were carried out on a horizontal bore 9.4T Biospec spectrometer using a linear coil for excitation and detection (Bruker BioSpin GmbH, Ettlingen, Germany), as previously reported [11,41,42]. Surrogate E6.5 pregnant mice carrying genetically modified embryos were serially scanned (each group consisted of 3-5 dams with 1-3 implantation sites). Mice were kept under respiratory monitoring while anesthetized by isoflurane (Abbott Laboratories, North Chicago, IL). The BSA-based macromolecular contrast material (biotin-bovine serum albumin (BSA)-GdDTPA; 80 kDa; r = 164 mM^{-1} s^{-1}; Symo-Chem, Eindhoven, Netherlands), was administered via a tail vein catheter as bolus at 10 mg/mouse in 0.2 mL of PBS. Series of variable-flip-angle precontrast T1-weighted 3D gradient-echo (3D-GE) images of the IS were acquired, before and sequentially 40 min after injecting the contrast agent. Variable flip angle pre-contrast T_1-weighted 3D-GE images were acquired to determine the pre-contrast R_1 (repetition time: 10 msec; echo time: 2.8 msec; flip angles: 5°, 15°, 30°, 50°, 70°; two averages; matrix: 256×256×64; field of view: 35×35×35 mm^3). The post-contrast images were obtained with a single flip angle (15°). Hyper permeable blood vessels were examined 40 min after biotin-BSA-GdDTPA injection (Figs 3G-3I, left side). Functional blood vessels were also confirmed in histological sections following IV injection of BSA labeled with 6-carboxy-X-rhodamine (BSA-ROX; 10 mg/mouse in 0.2 mL of PBS), 2 min before sacrificing the mice (Figs 3G-3I, right side). BSA was labeled with rhodamine 5(6)-carboxy-X-rhodamine succinimidyl ester (BSA-ROX; Molecular Probes, Eugene, OR) as reported previously [43], producing a labeling ranged between 2–4 fluorophores per protein molecule. Change in contrast agent concentration in the region of interest over time (C_t) was divided by its blood concentration (C_{blood}; extrapolated from vena cava region as time 0). Linear regression of these

temporal changes in C_t/C_{blood} yielded two vascular parameters: Fractional blood volume ($fBV=C_0/C_{blood}$) describes blood vessel density and is derived from the extrapolated concentration of the contrast agent in the IS at time zero, divided by the measured concentration in the vena cava, approximately 5 min after IV administration. Permeability surface area product ($PS=(C_t - C_0)/(C_{blood}\times t)$) depicting rate of contrast agent extravasation from blood vessels and its accumulation in the interstitial space, was derived from the slope of the linear regression of the first 15 min after contrast material administration (t=15). Mean fBV and PS were calculated separately for single IS.

Statistical analysis

All experiments were repeated at least 3 times using GraphPad Prism software version 8.0.0 for Windows (GraphPad Software, San Diego, CA, USA, www.graphpad.com). Statistically significant differences between experimental groups were analyzed with non-parametric post hoc test (Tukey-Kramer), as it was not normally distributed according to the Shapiro-Wilk test. The number of dams and implantation sites of each experiment indicated accordingly. Data is presented as mean ± SD with P values < 0.05 considered significant.

Results

TG expression and enzymatic activity in embryo implantation sites

Implantation sites (IS) at E5.5 (Fig 1) and E6.5 (Fig 2) were characterized for the localization and activity of TG2 and FXIII. At E5.5, TG2 was detected in TC (Fig 1A) while FXIII was detected within the implantation chamber (Fig 1E). TG2 and FXIII activity *in vivo* was assessed on frozen sections derived from IS following IV injection of T29-B (Fig 1B) or F11-B (Fig 1F) to E5.5 pregnant mice. Total TG2 and FXIII activities was detected *in situ* by exposing fresh sections of non-treated IS to T29-B (Fig 1C) or F11-B (Fig 1G). Negative controls for T29-B (Fig 1D) or F11-B (Fig 1H) showed inconsiderable signals upon *in situ* labelling with secondary antibodies without the SAs presence. On IS retrieved from E6.5 pregnant mice, TG2 (Fig 2A) or FXIII (Fig 2E) were further detected on the secondary decidual zone contra-position the mesometrial side. Similar distribution pattern of T29-B (Figs 2B,C) or F11-B (Figs 2F,G) on E6.5 IS was detected, after both IV *in vivo* and *in situ* administration of the SA. Non-specific incorporation of T29-B (Fig 2D) or F11-B (Fig 2H) was negligible as demonstrated *in situ* using the TG inhibitor iodoacetamide. Comparison of IS on E5.5 and E6.5 revealed substantial changes in TG2 and FXIII localizations. While on E5.5, TG2 and FXIII were mainly localized around the embryo, their expression shifted toward the mesometrial side, concentrating at the IS boundaries. Interestingly, FXIII localization in IS on E5.5 was associated within cell nuclear surrounding the embryo. This unexpected association was not detected on E6.5.

MRI reveals a role for TG2 and FXIII in maternal angiogenesis during embryo implantation

The role of TG2 and FXIII with decidual vascular remodeling was examined by DCE-MRI of E6.5 surrogate pregnant mice carrying embryos with transgenic trophectoderm induced by lentiviral infection of blastocysts. Significantly low permeability surface area product (PS, Fig J) values, consistent with attenuated extravasation of the MRI contrast agent, were measured in the IS with TC overexpressing FXIII (Figs 3B,E) but not overexpressing TG2 (Figs 3A,D) relative to the control group (Figs 3C,F). Fractional blood volume (fBV; Fig 3K), was reduced significantly at IS of embryos with TC overexpressing either FXIII or TG2. Accordingly, decreased histological labeling of biotin-BSA-GdDTPA was observed in IS with overexpressing TG2- (Fig 3G, left) or FXIII- (Fig 3H, left) TC, compared to IS with control vector (3I, left). As opposed to IS sections with TC overexpressing TG2 (Fig 3G, right) or

those expressing the control vector (Fig 3I, right), fluorescent BSA (BSA-ROX) was hardly detected in IS with FXIII-overexpressing TC (Fig 3H, right). PS values (Fig J) calculated from IS in which either TG2 (Figs 4A,D) or FXIII (Figs 4B,E) were depleted from TC using lentiCRISPR v2 lentiviral vector were not significantly different from the control (Figs 4C,F). A significant increase in PS values was measured from IS with FXIII-depleted TC (Fig 4K) relative to the control IS and also to the values calculated from IS with TG2-depleted TC. While IS with TG2-depleted TC (Fig 4K) revealed no significant changes compared to the control values. Histological cross sections of these IS were used to corroborate the changes in blood volume and permeability detected by the MRI. In IS with TG2-depleted TC (Fig 4G, left), biotin-BSA-GdDTPA was mainly distributed in the secondary decidual zone. Slight reduction in BSA-ROX distribution was observed in IS with TG2-depleted TC (Fig 4G, right) as compared to the control group (Fig 4I, right). Interestingly, the contrast agent was clearly detected in the embryonic niche of IS with FXIII-depleted TC (Fig 4H). IS vasculature was further characterized by CD34 staining for angiogenic neovasculature (Fig 5). CD34 in control IS (Figs 5A,C,E,G) was distributed in a mesh-like pattern, arrayed intensely on the anti-mesometrial region. Vessels expressing CD34 were detected in IS with TC overexpressing TG2 (Fig 5B) or TG2-depleted TC (Fig 5D). The organized vascular structure visualized by CD34 labeling of the control IS (Fig 5E), could not be detected on IS with TC overexpressing FXIII (Fig 5F). CD34 staining was elevated in IS with FXIII-depleted TC (Fig 5H) relative to control (Fig 5G). Quantitative analysis of the detected CD34 signal intensity, showed no significant difference between IS with TC overexpressing TG2 (Fig. 5I) or TG2-depleted TC (Fig 5J) compared to control sections. However, IS with TC overexpressing FXIII (Fig 5K) demonstrated a significant lower signal intensity while, IS with FXIII-depleted TC (Fig 5K) had significant higher signal intensity than their control.

Fibrinogen and Collagen IV remodeling is mediated by FXIII During Implantation

Fibrinogen was clearly detected in the anti-mesometrial pole and adjacent to control embryonic TC (Fig V.A, upper part). Increased fibrinogen deposition was detected in IS of FXIII overexpressing TC, particularly in the IS circumference, while fibrinogen was diminished at the embryonic vicinity (Fig V.B, upper part), as compared to control. Collagen IV (CIV) localization on the control IS (Fig V.A, lower part) was confined to the anti-mesometrial pole and around the primary decidual zone, while a substantial wider partition was displayed on the FXIII overexpressed TC (Fig V.B, lower part). Inversely to the IS with FXIII overexpressed TC, fibrinogen and CIV were hardly detected in IS with FXIII-depleted TC (Fig V.D) relative to control (Fig V.C).

Discussion

In this study, MRI was applied for detection of the role of the two TG isoenzymes, TG2 and FXIII, in decidual angiogenesis during early embryo implantation (Fig 6). TG2 and FXIII were expressed mostly at the feto-maternal interface and at the decidual anti-mesometrial pole at E5.5. and E6.5. Association between FXIII localization to cell nuclei was observed in the IS. Beyond the role of secreted FXIII in coagulation, it also mediates intranuclear crosslinking [44]. The role of TG isoenzymes on implantation was determined by manipulating TG2 and FXIII expression in embryonic TC. DCE-MRI showed reduced decidual vascular density in IS with TC overexpressing TG2, and elevated permeability in IS with TG2-depleted TC (Fig 6B). Decidual vasculature did not show significant changes when TG2 was depleted from TC. DCE-MRI revealed that TC derived FXIII regulates decidual vascular density. Substantially low fBV as well as low PS values were detected in IS where the TC overexpressed FXIII. IS with FXIII-depleted TC showed increased transcapillary leakage with higher PS values (Fig 6C) than IS of embryonic TC infected with an empty control vector (Fig 6A). Embryo implantation failure

is the primary cause for the low success of in vitro fertilization programs[5]. Impaired uterine hyper-permeability has been widely proposed as an important cause for implantation failure in humans[45].Several complications of pregnancy, such as preeclampsia and intrauterine growth restriction, have been attributed to disturbances in early uterine blood supply[13]or impaired trophoblast invasion of the placental bed spiral arterioles later in pregnancy[14].Therefore, it is important to characterize the processes regulating uterine ECM remodeling and angiogenesis during implantation, and MRI (specifically DCE-MRI) is a powerful tool addressing research requirements.

In our study, fibrinogen appeared to be diminished at the feto-maternal interface of the FXIII overexpressed IS, while it was increased on the decidua circumference. On the other hand, CIV was highly detected in IS with FXIII overexpressed TC extending further into the decidua, while it was narrowly confined around the control's embryo. Both fibrinogen and CIV were hardly detected in the IS with FXIII-depleted TC. Our findings indicate that enhanced activity of FXIII is associated with CIV presence. The precise role of FXIII in changing the fibrinogen distribution pattern is unclear. It is possible that FXIII and CIV take part in anchoring the embryo to the endometrium as suggested by Asahina [46].

Association between abnormal expression levels of TG2 or FXIII (CD) to both reduced fertility and increased risk of adverse pregnancy-related events has been long documented [47,48]. The activities of TG2 and FXIII were evaluated here using novel selective substrate analogs, T29-B and F11-B, respectively, suggesting their potential as molecular imaging probes in selective detection of TG2 and FXIII. TG isoenzyme localization showed a direct correlation to their SA distribution. Establishment of implantation sites with genetically modified TC, enabled us to study the effect on maternal angiogenesis upon TG2 and FXIII modulation. Our findings demonstrated that TC derived TG2 plays an important role in regulating decidual vascular permeability, while TC derived FXIII regulates vascular density as well as permeability. These findings suggest distinct roles for TG2 and FXIII during embryo implantation and may shed light on TG-reduced fertility. Moreover, MRI provides a modality of choice for high resolution in vivo imaging of the early stages of pregnancy, and particularly the maternal angiogenesis induced by the implanting embryo.

Acknowledgments

Michal Neeman is incumbent of the Helen and Morris Mauerberger Chair in Biological Sciences. GC, RH, RS, AP, DL, ME performed experiments and analyzed data. SB analyzed data. FK assisted in protocol design. GC, RH, ND, EG SA and MN designed the study and wrote the paper.

Sources of funding

This work was supported by the Seventh Framework European Research Council Advanced Grant 232640-IMAGO and by National Institutes of Health (grant 1R01HD086323).

Disclosure

The authors declare that they have no conflict of interest.

References

1. Zhang S, Lin H, Kong S, Wang S, Wang HH, Wang HH, Armant DR. Physiological and molecular determinants of embryo implantation. *Mol Aspects Med*. 2013;34:939-980. doi:10.1016/j.mam.2012.12.011.Physiological.
2. Dey SK, Lim H, Das SK, Reese J, Paria BC, Daikoku T, Wang H. Molecular cues to implantation. *Endocr Rev*. 2004;25:341-373. doi:10.1210/er.2003-0020.
3. Welsh AO, Enders AC. Chorioallantoic placenta formation in the rat: I. luminal epithelial cell death and extracellular matrix modifications in the mesometrial region of implantation chambers. *Am J Anat*. 1991;192:215-231.

doi:10.1002/aja.1001920302.
4. Welsh AO, Enders AC. Chorioallantoic placenta formation in the rat: II. angiogenesis and maternal blood circulation in the mesometrial region of the implantation chamber prior to placenta formation. *Am J Anat*. 1991;192:347-365. doi:10.1002/aja.1001920404.
5. Cha J, Sun X, Dey SK. Mechanisms of implantation: strategies for successful pregnancy. *Nat Med*. 2012;18:1754-1767. doi:10.1038/nm.3012.
6. Sharkey AM, Smith SK. The endometrium as a cause of implantation failure. *Best Pract Res Clin Obstet Gynaecol*. 2003;17:289-307. doi:10.1016/S1521-6934(02)00130-X.
7. Georgiades P, Cox B, Gertsenstein M, Chawengsaksophak K, Rossant J. Trophoblast-specific gene manipulation using lentivirus-based vectors. *Biotechniques*. 2007;42:317-325. doi:10.2144/000112341.
8. Carson DD, Bagchi I, Dey SK, Enders AC, Fazleabas AT, Lessey BA, Yoshinaga K. Embryo implantation. *Dev Biol*. 2000;223:217-237. doi:10.1006/dbio.2000.9767.
9. Matsumoto H, Ma WG, Daikoku T, Zhao X, Paria BC, Das SK, Trzaskos JM, Dey SK. Cyclooxygenase-2 differentially directs uterine angiogenesis during implantation in mice. *J Biol Chem*. 2002;277:29260-29267. doi:10.1074/jbc.M203996200.
10. Plaisier M. Decidualisation and angiogenesis. *Best Pract Res Clin Obstet Gynaecol*. 2011;25:259-271. doi:10.1016/j.bpobgyn.2010.10.011.
11. Plaks V, Birnberg T, Berkutzki T, Sela S, BenYashar A, Kalchenko V, Mor G, Keshet E, Dekel N, Neeman M, Jung S. Uterine DCs are crucial for decidua formation during embryo implantation in mice. *J Clin Invest*. 2008;118:3954-3965. doi:10.1172/JCI36682.
12. Quenby S, Farquharson RG, Dawood F, Hughes AM, Topping J. Recurrent miscarriage and long-term thrombosis risk: a case-control study. *Hum Reprod*. 2005;20:1729-1732. doi:10.1093/humrep/deh844.
13. Redman CW, Sargent IL. Latest advances in understanding preeclampsia. *Science*. 2005;308:1592-1594. doi:10.1126/science.1111726.
14. Hanna J, Goldman-Wohl D, Hamani Y, et.al. Decidual NK cells regulate key developmental processes at the human fetal-maternal interface. *Nat Med*. 2006;12:1065-1074. doi:10.1038/nm1452.
15. Eckert RL, Kaartinen MT, Nurminskaya M, Belkin AM, Colak G, Johnson GVW, Mehta K. Transglutaminase regulation of cell function. *Physiol Rev*. 2014;94:383-417. doi:10.1152/physrev.00019.2013.
16. Wang Z, Perez M, Caja S, Melino G, Johnson TS, Lindfors K, Griffin M. A novel extracellular role for tissue transglutaminase in matrix-bound VEGF-mediated angiogenesis. *Cell Death Dis*. 2013;4:e808. doi:10.1038/cddis.2013.318.
17. Kabir-salmani M, Shiokawa S, Akimoto Y, Sakai K, Sakai K, Iwashita M. Tissue transglutaminase at embryo-maternal interface. *J Clin Endocrinol Metab*. 2005;90:4694-4702. doi:10.1210/jc.2005-0240.
18. Dickneite G, Herwald H, Korte W, Allanore Y, Denton CP, Cerinic MM. Coagulation factor XIII: a multifunctional transglutaminase with clinical potential in a range of conditions. *Thromb Haemost*. 2015;113:686-697. doi:10.1160/TH14-07-0625.
19. Siebenlist K, Meh D, Mosesson M. Protransglutaminase (factor XIII) mediated crosslinking of fibrinogen and fibrin. *Thromb Haemost*. 2001;86:1221-1228. doi:10.1055/s-0037-1616055.
20. Procyk R, Blomback B. Factor XIII-induced crosslinking in solutions of fibrinogen and fibronectin. *Biochim Biophys Acta*. 1988;967:304-313. doi:10.1016/0304-4165(88)90024-4.

21. Prince CW, Dickie D, Krumdieck CL. Osteopontin, a substrate for transglutaminase and factor XIII activity. *Biochem Biophys Res Commun*. 1991;177:1205-1210. doi:10.1016/0006-291X(91)90669-X.
22. Lynch GW, Slayter HS, Miller BE, McDonagh J. Characterization of thrombospondin as a substrate for factor XIII transglutaminase. *J Biol Chem*. 1987;262:1772-1778.
23. Tei L, Mazooz G, Shellef Y, Avni R, Vandoorne K, Barge A, Kalchenko V, Dewhirst MW, Chaabane L, Miragoli L, Longo D, Neeman M, Aime S. Novel MRI and fluorescent probes responsive to the factor XIII transglutaminase activity. *Contrast Media Mol Imaging*. 2010;5:213-222. doi:10.1002/cmmi.392.
24. Mazooz G, Mehlman T, Lai T, Greenberg CS, Dewhirst MW, Neeman M. Development of magnetic resonance imaging contrast material for in vivo mapping of tissue transglutaminase activity. *Cancer Res*. 2005;65:1369-1375. doi:10.1158/0008-5472.CAN-04-2269.
25. Hitomi K, Kitamura M, Sugimura Y. Preferred substrate sequences for transglutaminase 2: screening using a phage-displayed peptide library. *Amino Acids*. 2009;36:619-624. doi:10.1007/s00726-008-0126-6.
26. Piacentini M, Autuori F. Immunohistochemical localization of tissue transglutaminase and Bcl-2 in rat uterine tissues during embryo implantation and post-partum involution. *Differentiation*. 1994;57:51-61. doi:10.1046/j.1432-0436.1994.5710051.x.
27. Sugimura Y, Hosono M, Wada F, Yoshimura T, Maki M, Hitomi K. Screening for the preferred substrate sequence of transglutaminase using a phage-displayed peptide library: identification of peptide substrates for TGASE 2 and Factor XIIIA. *J Biol Chem*. 2006;281:17699-17706. doi:10.1074/jbc.M513538200.
28. Sugimura Y, Ueda H, Maki M, Hitomi K. Novel site-specific immobilization of a functional protein using a preferred substrate sequence for transglutaminase 2. *J Biotechnol*. 2007;131:121-127. doi:10.1016/j.jbiotec.2007.05.037.
29. Sugimura Y, Hosono M, Kitamura M, Tsuda T, Yamanishi K, Maki M, Hitomi K. Identification of preferred substrate sequences for transglutaminase 1 - development of a novel peptide that can efficiently detect cross-linking enzyme activity in the skin. *FEBS J*. 2008;275:5667-5677. doi:10.1111/j.1742-4658.2008.06692.x.
30. Kawamoto T, Shimizu M. A method for preparing 2- to 50-micron-thick fresh-frozen sections of large samples and undecalcified hard tissues. *Histochem Cell Biol*. 2000;113:331-339. doi:10.1007/s004180000149.
31. Itoh M, Tatsukawa H, Eun-Seo L, Yamanishi K, Kojima S, Hitomi K. Variations in both TG1 and TG2 isozyme-specific in situ activities and protein expressions during mouse embryonic development. *J Histochem Cytochem*. 2013;61:793-801. doi:10.1369/0022155413501676.
32. Rhee JM, Pirity MK, Lackan CS, Long JZ, Kondoh G, Takeda J, Hadjantonakis AK. In vivo imaging and differential localization of lipid-modified GFP-variant fusions in embryonic stem cells and mice. *Genesis*. 2006;44:202-218. doi:10.1002/dvg.20203.
33. Hsu PD, Scott DA, Weinstein JA, Ran FA, Konermann S, Agarwala V, Li Y, Fine EJ, Wu X, Shalem O, Cradick TJ, Marraffini LA, Bao G, Zhang F. DNA targeting specificity of RNA-guided Cas9 nucleases. *Nat Biotechnol*. 2013;31:827-832. doi:10.1038/nbt.2647.
34. Doench JG, Hartenian E, Graham DB, Tothova Z, Hegde M, Smith I, Sullender M, Ebert BL, Xavier RJ, Root DE. Rational design of highly active sgRNAs for CRISPR-Cas9-mediated gene inactivation. *Nat Biotechnol*. 2014;32:1262-1267. doi:10.1038/nbt.3026.
35. Doench JG, Fusi N, Sullender M, Hegde M, Vaimberg EW, Donovan KF, Smith I, Tothova Z, Wilen C, Orchard R, Virgin HW, Listgarten J, Root DE. Optimized

sgRNA design to maximize activity and minimize off-target effects of CRISPR-Cas9. *Nat Biotechnol*. 2016;32:184-191. doi:10.1038/nbt.3437.
36. Xu H, Xiao T, Chen CH, Li W, Meyer CA, Wu Q, Wu D, Cong L, Zhang F, Liu JS, Brown M, Liu XS. Sequence determinants of improved CRISPR sgRNA design. *Genome Res*. 2015;25:1147-1157. doi:10.1101/gr.191452.115.
37. Chari R, Mali P, Moosburner M, Church GM. Unraveling CRISPR-Cas9 genome engineering parameters via a library-on-library approach. *Nat Methods*. 2015;12:823-826. doi:10.1038/nmeth.3473.
38. Sanjana NE, Shalem O, Zhang F. Improved vectors and genome-wide libraries for CRISPR screening. *Nat Methods*. 2014;11:783-784. doi:10.1038/nmeth.3047.
39. Regev L, Neufeld-Cohen A, Tsoory M, Kuperman Y, Getselter D, Gil S, Chen A. Prolonged and site-specific over-expression of corticotropin-releasing factor reveals differential roles for extended amygdala nuclei in emotional regulation. *Mol Psychiatry*. 2011;16:714-728. doi:10.1038/mp.2010.64.
40. Kumasawa K, Ikawa M, Kidoya H, Hasuwa H, Saito-fujita T. Pravastatin induces placental growth factor (PGF) and ameliorates preeclampsia in a mouse model. *Proc Natl Acad Sci U S A*. 2011;108:1451-1455. doi:10.1073/pnas.1011293108.
41. Plaks V, Kalchenko V, Dekel N, Neeman M. MRI analysis of angiogenesis during mouse embryo implantation. *Magn Reson Med*. 2006;55:1013-1022. doi:10.1002/mrm.20881.
42. Plaks V, Gershon E, Zeisel A, Jacob-hirsch J, Neeman M, Winterhager E, Rechavi G, Domany E, Dekel N. Blastocyst implantation failure relates to impaired translational machinery gene expression. *Reproduction*. 2014;148:87-98. doi:10.1530/REP-13-0395.
43. Dafni H, Gilead A, Nevo N, Eilam R, Harmelin A, Neeman M. Modulation of the pharmacokinetics of macromolecular contrast material by avidin chase: MRI, optical, and inductively coupled plasma mass spectrometry tracking of triply labeled albumin. *Magn Reson Med*. 2003;50:904-914. doi:10.1002/mrm.10638.
44. Ádány R, Bárdos H, Antal M, Módis L, Sárváry A, Szücs S, Balogh I. Factor XIII of blood coagulation as a nuclear crosslinking enzyme. *Thromb Haemost*. 2001;85:845-851. doi:10.1055/s-0037-1615758.
45. Pulendran B, Smith JL, Caspary G, Brasel K, Pettit D, Maraskovsky E, Maliszewski CR. Distinct dendritic cell subsets differentially regulate the class of immune response in vivo. *Proc Natl Acad Sci U S A*. 1999;96:1036-1041. doi:https://doi.org/10.1073/pnas.96.3.1036.
46. Asahina T, Kobayashi T, Okada Y, Itoh M, Yamashita M, Inamoto Y, Terao T. Studies on the role of adhesive proteins in maintaining pregnancy. *Horm Res Paediatr*. 1998;50:37-45. doi:10.1159/000053122.
47. Di Simone N, Silano M, Castellani R, Di Nicuolo F, D'Alessio MC, Franceschi F, Tritarelli A, Leone AM, Tersigni C, Gasbarrini G, Silveri NG, Caruso A, Gasbarrini A. Anti-tissue transglutaminase antibodies from celiac patients are responsible for trophoblast damage via apoptosis in vitro. *Am J Gastroenterol*. 2010;105:2254-2261. doi:10.1038/ajg.2010.233.
48. Dorgalaleh A, Rashidpanah J. Blood coagulation factor XIII and factor XIII deficiency. *Blood Rev*. 2016;30:461-475. doi:10.1016/j.blre.2016.06.002.

Highlights

- TG2 and FXIII transglutaminases are active in the embryo implantation site in mice.
- Modulation of trophoblast TG2 or FXIII expression alters maternal angiogenesis.

- TG modulation maternal angiogenesis in implantation is detectable by MRI.

Figures and Figure legends

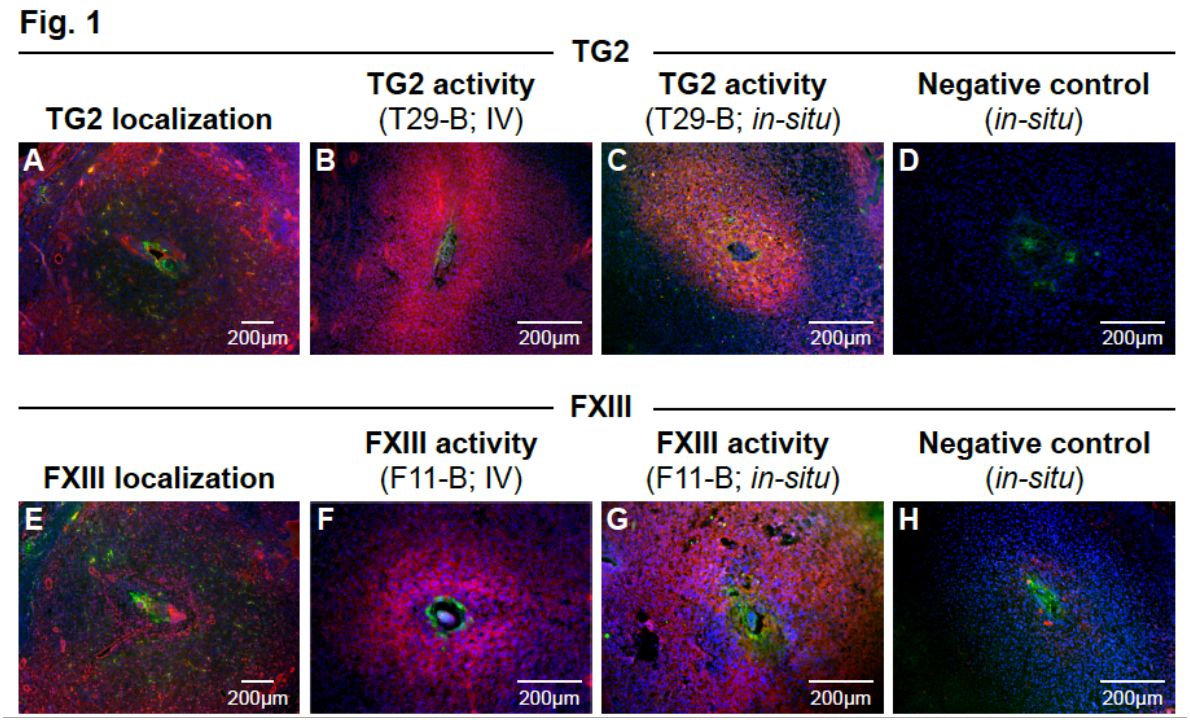

Figure 1. TG2 and FXIII activities, detected by SAs distribution, resemble their localization in ISs retrieved from E5.5 pregnant C57bl/6J mice. Myr-Venus homozygote males) were mated with C57bl/6J female mice, producing hemizygote Myr-Venus embryos. **A**. TG2 localization in paraffin sections of embryo IS. Red represents antibody staining for TG2 (4 dams, 20 ISs); **B, C.** TG2 activity, detected by T29-B distribution 45 min after it was injected IV (**B**, 4 dams, 14 ISs) or applied *in situ* on live sections (**C**, 4 dams, 16 ISs). For images **B** and **C**, red represents T29-B distribution, followed by Cy3-streptavidin staining; **D**. Negative control sections stained with Cy3-streptavidin staining without T29-B SA (5 dams, 20 ISs); **E**. FXIII distribution in paraffin sections of embryo IS (4 dams, 20 ISs). Red represents antibody staining for FXIII; **F, G.** FXIII activity, detected by F11-B distribution 45 min after it was injected IV (**F**, 5 dams, 17 ISs) or applied *in situ* on live sections **(G**, 4 dams, 11 ISs**)**. For images **F** and **G**, red represents F11-B distribution, following Cy3-streptavidine staining; **H**. Negative control sections stained with Cy3-streptavidin staining without F11-B SA (5 dams, 20 ISs). For all images: green represents hemizygote Myr-Venus embryos; blue DAPI staining. Image scale bars are 200 µm.

Fig. 2

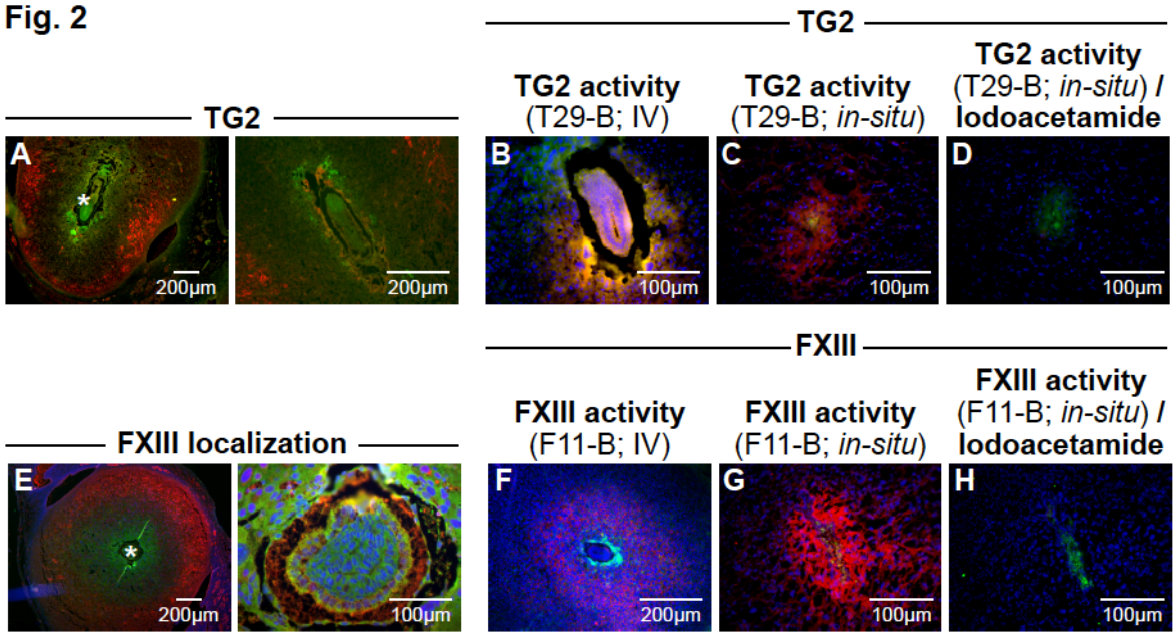

Figure 2. TG2 and FXIII specific activities matched their localization on the feto-maternal interface of ISs retrieved from E6.5 pregnant C57bl/6J mice. Myr-Venus homozygote males were mated with C57bl/6J female mice, producing hemizygote Myr-Venus embryos. **A**. **Left,** TG2 localization in paraffin sections of embryo IS**.** Red represent antibody for TG2. * Estimated embryonic region. **Right**, magnification of the marked region (3 dams, 24 ISs); TG2 activity, detected by T29-B distribution 45 min after it was injected IV **(B**, 3 dams, 13 ISs) or applied *in situ* on live sections (**C**, 4 dams, 18 ISs); **D**. TG2 specific activity, detected *in situ* on live sections after T29-B was applied in the presence of TG inhibitor, Iodoacetamide. For images **B, C** and **D**, red represents T29-B distribution, following Cy3-streptavidin staining (4 dams, 16 ISs); **E**. **Left**, FXIII localization in paraffin sections of embryo IS. Red represents antibody for FXIII. * Estimated embryonic region. **Right**, magnification of the marked region (4 dams, 28 ISs); FXIII activity, detected by F11-B distribution 45 min after it was injected IV (**F**, 5 dams, 24 ISs) or applied *in situ* on live sections (**G**, 5 dams, 20 ISs); **H**. FXIII specific activity, detected *in situ* on live sections after F11-B was applied in the presence of Iodoacetamide (4 dams, 16 ISs). For images **F, G** and **H**, red represents F11-B distribution, following Cy3-streptavidin staining. For all images: green represents hemizygote Myr-Venus embryos; DAPI in blue. Images scale bars are 100 or 200 µm.

Fig. 3

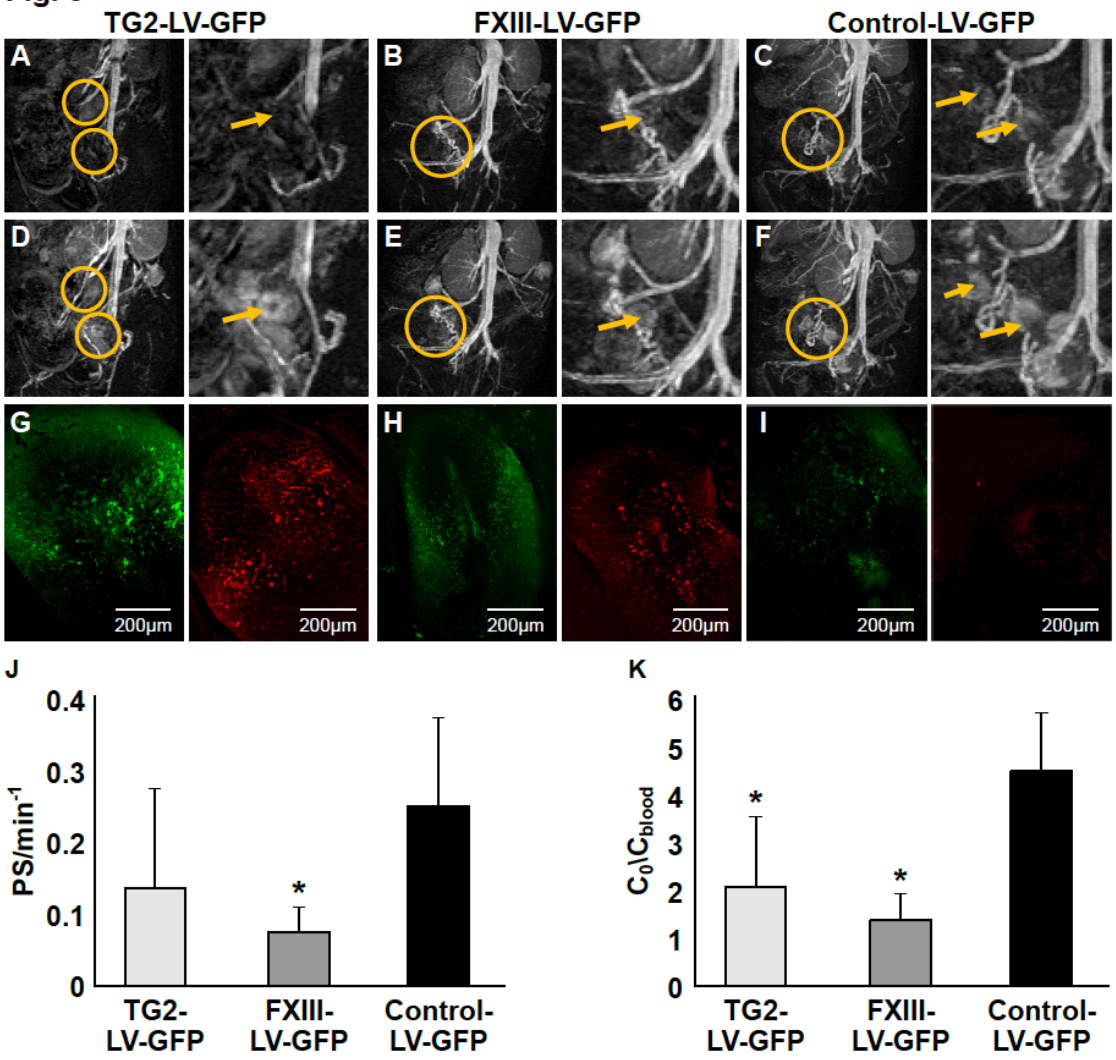

Figure 3. Impaired decidual vascular function of ISs with genetically modified TC overexpressing TG2 or FXIII. T1 weighted gradient-echo images acquired from surrogate E6.5 pregnant ICR mice carrying transgenic embryonic TC overexpressing TG2 (**A, D**; TG2-LV-GFP), overexpressing FXIII (**B, E**; FXIII-LV-GFP) or expressing the control vector (**C, F**; Control-LV-GFP), 3 min (**A, B, C**) or 40 min (**D, E, F**) after biotin-BSA-GdDTPA injection. Individual ISs are indicated by orange circles. Right, magnification of the adjacent left image; Validation of the decidual blood vessels permeability functions by visualizing biotin-BSA-GdDTPA distribution in paraffin sections of ISs with transgenic embryonic TC overexpressing TG2 (**G, Left**), overexpressing FXIII (**H, Left**) or expressing the control vector (**I, Left**). Green represent contrast agent distribution, 40 min after it was injected, using streptavidin-Cy2 staining; Validation of functional decidual blood vessels by detecting BSA-ROX distribution in paraffin sections of ISs with transgenic embryonic TC overexpressing TG2 (**G, Right**), overexpressing FXIII (**H, Right**) or expressing the control vector (**I, Right**). Red represents the distribution of BSA-ROX, 2 min after it was injected; Quantitative analysis of vessel density and vascular permeability in the ISs using the MRI parameters: permeability surface area product (**J**) and fraction blood volume (**K**). The values are calculated as mean ± SD of transgenic embryos overexpressing TG2 (4 dams, 12 ISs), overexpressing FXIII (5 dams, 19 ISs) or expressing the control vector (5 dams, 13 ISs). * $p<0.05$ *vs* Control-LV-GFP. Image scale bars are 200 µm.

Fig. 4

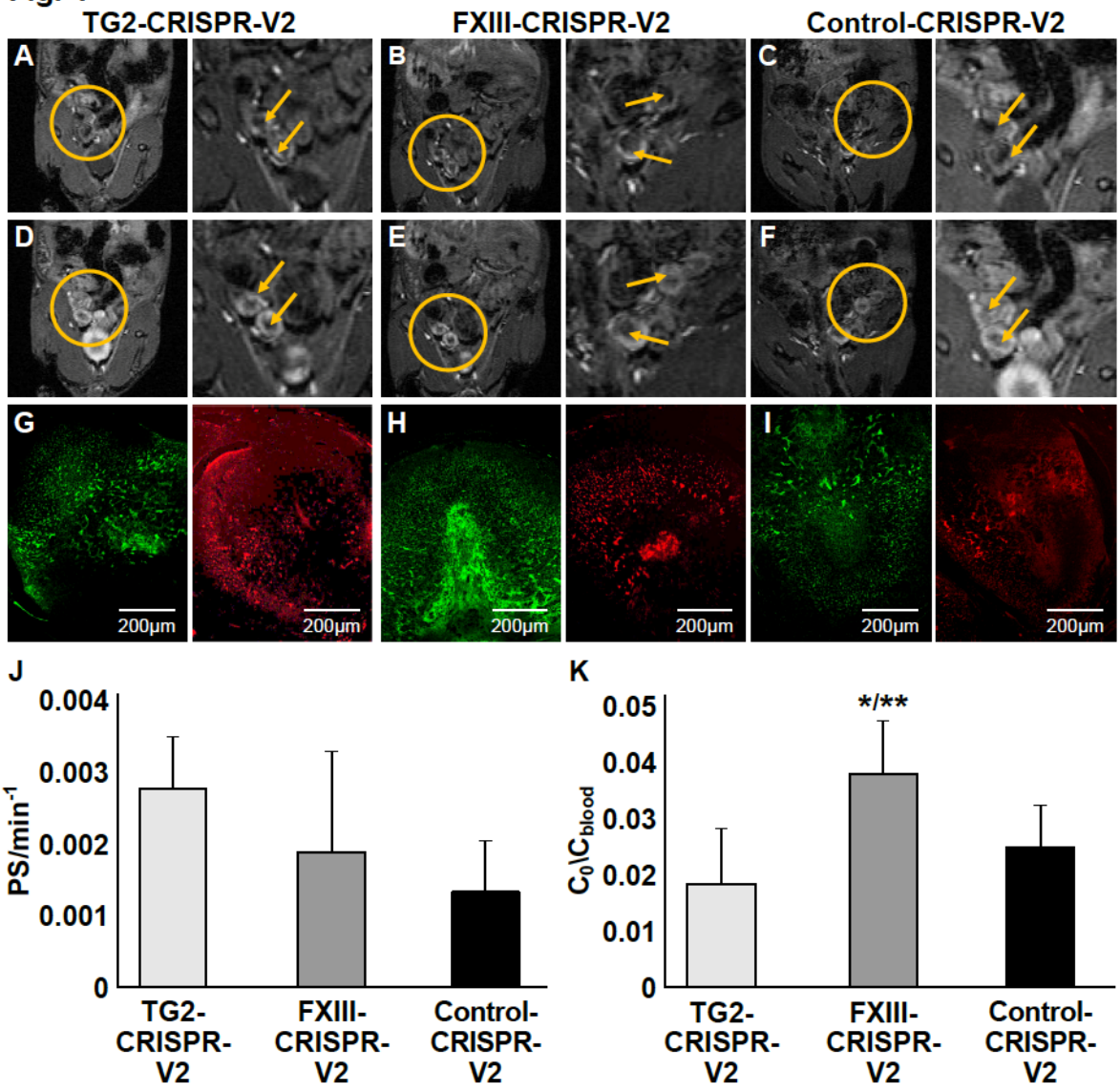

Figure 4. Decidual blood vessel function increased in ISs with TG2- or FXIII-depleted embryonic TC. T1 weighted gradient-echo images acquired from surrogate pregnant ICR mice carrying embryos with genetically modified TC depleted from TG2 (**A, D**; TG2-CRISPR-V2), depleted from FXIII (**B, E**; FXIII-CRISPR-V2) or expressing the control vector (**C, F**; Control-CRISPR-V2), 3 min (**A, B, C**) or 40 min (**D, E, F**) after biotin-BSA-GdDTPA injection. Individual ISs are indicated by orange circles. Right side, magnification of the adjacent left image; Validation of the decidual blood vessels permeability by visualizing biotin-BSA-GdDTPA distribution in paraffin sections of ISs with embryonic TC depleted from TG2 (**D, Left**; TG2-CRISPR-V2), depleted from FXIII (**E, Left**; FXIII-CRISPR-V2) or expressing the control vector (**F, Left**; Control-CRISPR-V2), Green represent the distribution of the contrast agent 40 min after injection using streptavidin-Cy2 staining; Validation of functional decidual blood vessels by detecting BSA-ROX distribution in paraffin sections of ISs with embryonic TC depleted from TG2 (**G, Right;** TG2-CRISPR-V2), depleted from FXIII (**H, Right;** FXIII-CRISPR-V2) or expressing the control vector (**I, Right;** Control-CRISPR-V2), Red represents the distribution of BSA-ROX injected 2 min before sacrificing the mouse; Quantitative analysis using the MRI parameters: permeability surface area product (**J**) and fraction blood volume (**K**). The values are calculated as mean ± SD of transgenic embryo models depleted from TG2 (3 dams, 10 ISs), FXIII (4 dams, 12 ISs) or expressing the control vector (4 dams, 9 ISs), PS:

* p<0.05 *vs* Control-CRISPR-V2; ** p<0.05 vs TG2-CRISPR-V2. Images scale bars are 200 µm.

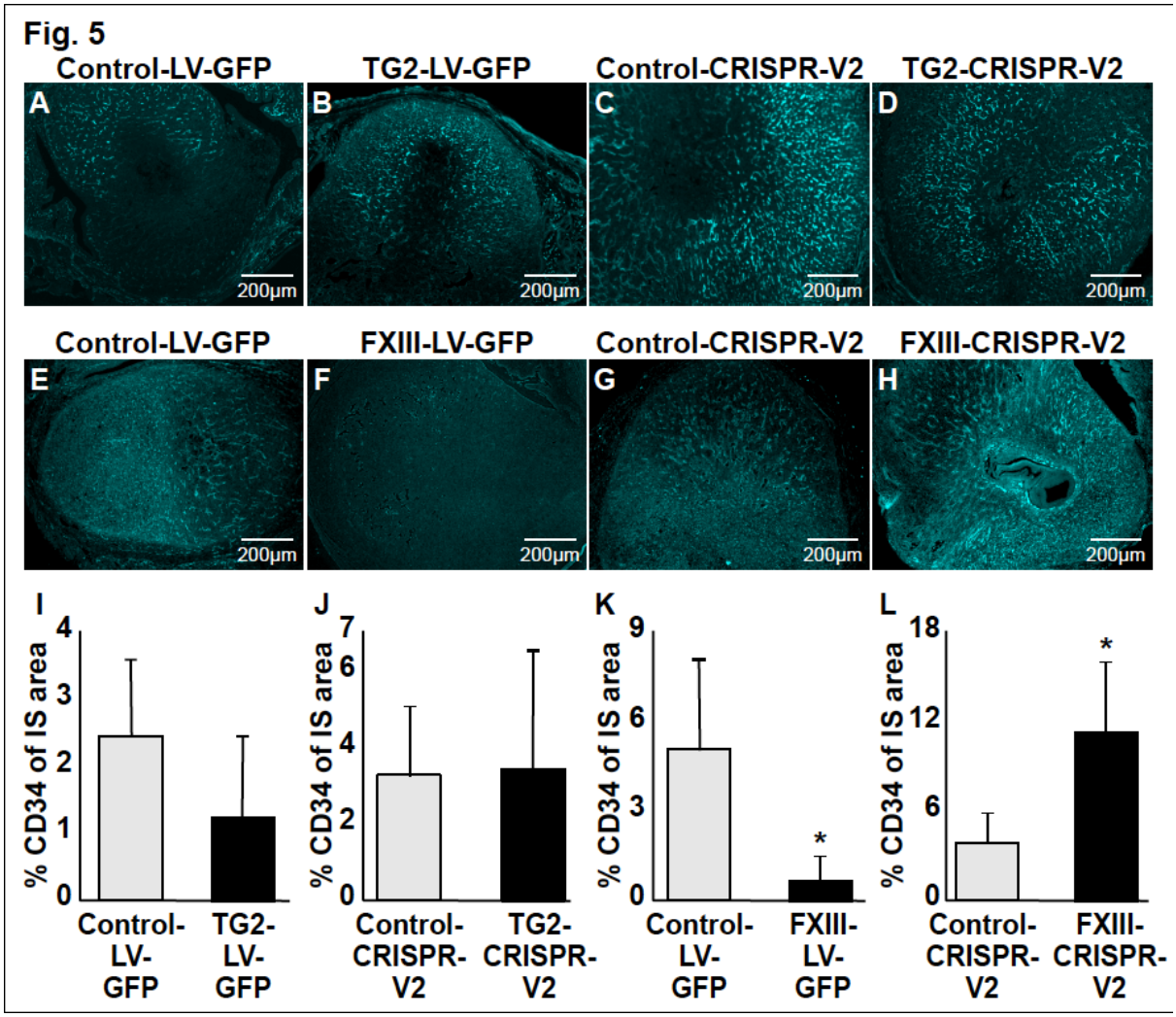

Figure 5. Microvascular evaluation of the ISs with transgenic embryos. Immunostaining for CD34 in ISs of genetically modified TC expressing the control vector (LV-GFP, **A** and **E;** CRISPR-V2, **C** and **G**, both 4 dams, 10 ISs), overexpressing TG2 (TG2-LV-GFP; **B**, 4 dams, 12 ISs), depleted from TG2 (**D**, 3 dams, 10 ISs), overexpressing FXIII (**F**, 5 dams, 19 ISs) or depleted from FXIII (**H**, 4 dams, 12 ISs). CD34 was visualized by cyan fluorescence channel after labeled with Cy5-avidin. Similar exposure time was used for each section and its appropriate control. Quantitative analysis of % CD34 staining in relation to IS area of genetically modified TC overexpressing TG2 (I), depleted from TG2 (**J**), overexpressing FXIII (**K**) or depleted from FXIII (**L**). Image scale bars are 200 µm. * p<0.05 *vs* Control-vector.

Fig. 6

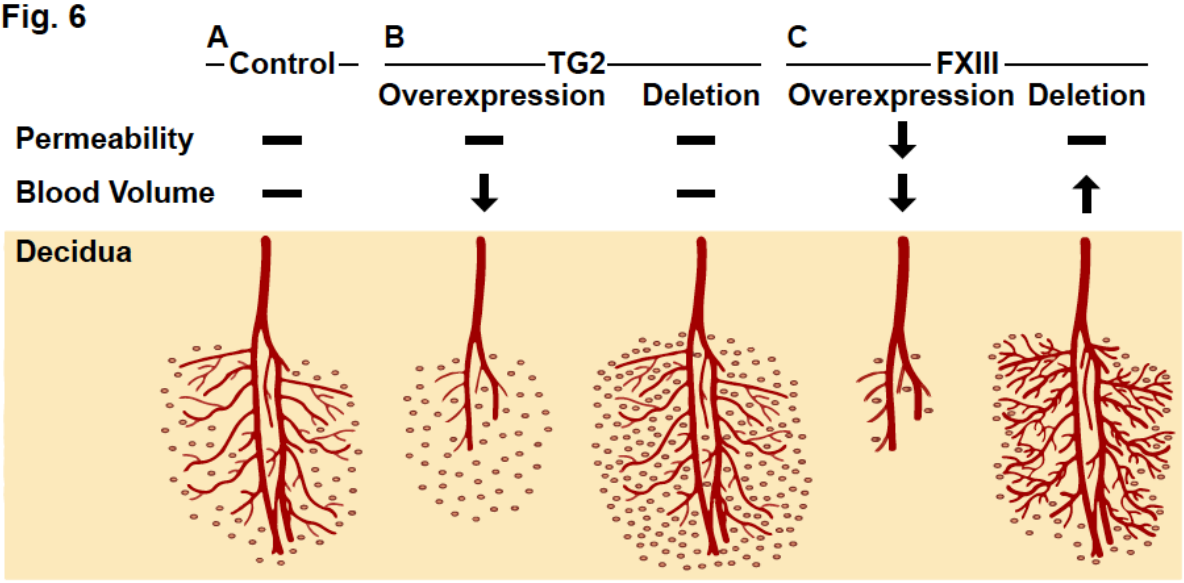

Figure 6. The effect of TC derived TG2 or FXIII on the decidual vascular function. **A**. Decidual blood vessels permeability and blood volume; Embryo TC infected by lenti virus to overexpressing TG2 (**B**, **Left**) or FXIII (**C**, **Left**), display a decrease in decidual blood volume. Overexpressing of FXIII also shows a significant decrease in decidual blood vessels permeability (**C**, **Left**); Decidual vasculature properties did not change when embryonic TC were depleted of TG2 (**B**, **Right**), while depletion of FXIII (**C**, **Right**) shows a significant increase in decidual blood volume. Red branched lines represent blood vessels density; ovals represent blood vessel permeability.